



Ultra-low dielectric constant fluorinated graphene/polybenzoxazole composite films with excellent thermal stabilities and mechanical properties

Zihua Yu^{a,b}, Shaohua Wu^{a,*}, Chuncheng Li^{a,*}, Yaonan Xiao^a, Liuchun Zheng^a, Jiajian Liu^a, Bo Zhang^a

^a Beijing National Laboratory for Molecular Sciences, Key Laboratory of Engineering Plastics, Institute of Chemistry, Chinese Academy of Sciences (ICCAS), Beijing 100190, PR China

^b University of the Chinese Academy of Sciences, Beijing 100049, PR China

ARTICLE INFO

Keywords:

- A. Polymer-matrix composites (PMCs)
- A. Thin films
- B. Electrical properties
- B. Thermal properties

ABSTRACT

Unsatisfied dielectric properties and inferior mechanical properties have become the main obstacles limiting the application of polybenzoxazole (PBO) in the field of microelectronics. Herein, a novel nanocomposite film was successfully developed by introducing fluorinated graphene (FG) into fluorinated PBO (FPBO). Interestingly, the FG/FPBO composite films showed an ultra-low dielectric constant of 2.02 at 1 MHz. Meanwhile, the tensile strength of the composite films increased up to 103.5 MPa, which was 25% higher than that of the pristine FPBO. Moreover, the 5% weight loss temperature of FG/FPBO composites were as high as 525 °C, displayed an outstanding heat resistance. The water absorption of FG/FPBO films have also dropped from 1% to 0.5% due to the high hydrophobicity of FG. In short, our work provides a simple and efficient approach for the preparation of high-performance films with low dielectric constant and water absorption, as well as high mechanical strength and thermal stability.

1. Introduction

With the rapid development of 5G communication technology, low dielectric constant (low- κ) materials have become a research focus due to their great effectiveness in reducing the resistance capacitance delay and the cross-talk noise between wires in integrated circuits [1–4]. Among various low- κ materials, polybenzoxazole (PBO) possesses excellent properties of high strength, high modulus, high heat resistance, low water absorption, and high chemical stability, being highly praised as key materials for the preparation of next-generation interlayer dielectrics [5–12]. However, the dielectric constant ($\kappa = 2.9\text{--}3.2$) of PBO [13] is still higher than the threshold ($\kappa \leq 2.3$) recommended in the International Technology Roadmap for Semiconductors (ITRS) [14]. Therefore, it is highly desirable to reduce the dielectric constant of PBO.

Reducing the polarizability or mass density are two general ways for reducing the dielectric constant of a material [13,15–18]. The reduction of mass density, which is achieved by introducing air ($\kappa = 1$), could greatly reduce the dielectric constant of PBO [19]. Rigid porous nanoparticles are often used to introduce air into the matrix due to their

controllable size and uniform distribution of pores. However, the significant reduction in the dielectric constant could only be achieved under a high loading content (10–20 wt%), which inevitably leads to severe aggregation of the nanoparticles and serious decrease in the mechanical properties of the resulting nanocomposites [20]. For instance, Zhou et al. [21] recently prepared a nanocomposite film with dielectric constant as low as 2.12 by incorporating a metal-organic framework material of ZIF-8 coated hollow silica into PBO. The tensile strength of the film dropped sharply from 68 to 34 MPa. On the contrary, lowering the polarizability by introducing fluorine-containing groups bring little damage to the intrinsic strength of PBO. In addition, the flexible fluorine-containing groups can also reduce the rigidity of the PBO molecular chain, thereby improving its processing performance [22]. Nevertheless, this strategy usually involves complicated synthetic routes, which greatly limits its practical application. Moreover, the fluorinated PBO (FPBO) previously reported has a low fluorine content, which contributes little to reducing the dielectric constant [23]. For example, Tao et al. [24] synthesized a series of FPBO by varying the fluorine content. However, the dielectric constants of these FPBO were

* Corresponding authors.

E-mail addresses: wushaohua12@iccas.ac.cn (S. Wu), lichch@iccas.ac.cn (C. Li).

relatively high ($\kappa = 2.5\text{--}2.7$) and failed to meet the requirements. Therefore, it remains a great challenge to effectively reduce the dielectric constant of PBO while maintaining its original excellent mechanical properties.

Recently, fluorinated graphene (FG), as a new derivative of graphene (GS), has attracted great attentions. The abundant fluorine atoms endow FG with many fascinating properties different from GS, such as ultra-low dielectric constant ($\kappa \approx 1.2$) [25–27]. FG has therefore become a very promising nanofiller candidate for the preparation of next-generation low- κ materials. However, to the best of our knowledge, there has been no report on the modification of PBO with FG. Besides, due to the extremely low surface energy of FG, uniformly dispersing FG in the PBO matrix will become an urgent problem to be solved [28,29].

In this work, a facile and versatile strategy was developed to effectively prepare PBO-based nanocomposite with outstanding properties, including mechanical properties, thermal stability, and dielectric properties. First, a high-molecular-weight fluorinated poly(hydroxyamide) (FPHA), i.e. the precursor of FPBO, was synthesized by using commercial fluoromonomer of 2,2-bis(3-amino-4-hydroxyphenyl) hexafluoropropane (6FAP). Subsequently, according to the principle of similar compatibility [30,31], FG was uniformly dispersed in FPHA by a simple solution blending method. Finally, FG/FPBO composite film could be obtained by thermal cyclization of FG/FPHA. Furthermore, the influence of the microstructure of FG/FPBO on its comprehensive performance was studied in detail.

2. Experimental

2.1. Materials

Graphite fluoride was purchased from Hubei Zhuoxi Fluorination Technology Co., Ltd. (China). 6FAP, terephthaloyl chloride (TPC), pyridine (anhydrous), and chlorotrimethylsilane (TMCS) was obtained from J&K Scientific Ltd. (China). Anhydrous 1-methyl-2-pyrrolidinone (NMP) was purchased from Beijing Innochem Science & Technology Co., Ltd. (China). Isopropanol (IPA) and methanol was provided by Concord

Technology Co., Ltd. (Tianjin, China). Before use, 6FAP and TPC were dried under vacuum at 30 °C for 12 h. Other reagents were used as received.

2.2. Preparation of FG

Graphite fluoride was exfoliated into FG by ultrasonic treatment according to previous reports [32]. In brief, 0.8 g of graphite fluoride was first dispersed in 100 mL of IPA, followed by sonicating at 100 W for 6–24 h. The suspension was centrifuged at 3000 rpm for 10 min to separate the unexfoliated graphite fluoride. The poor solubility of FPHA in IPA hindered the subsequent preparation of FG/FPBO composite films. Thus, 20 mL of NMP was added in the supernatant and replaced IPA by vacuum distillation at 40 °C for 30 min.

2.3. Synthesis of FPHA

The FPHA was synthesized by a silylation method as depicted in Fig. 1 a. Typically, 6FAP (2.80 g) was first dissolved in 20 mL of anhydrous NMP by mechanical stirring at room temperature. TMCS (3.9 mL) and pyridine (3.2 mL) were added to above solution and stirred for 2 h to protect the hydroxy groups. Then the system was cooled to 0 °C in an ice-water bath before TPC (1.55 g) was added. After that, the reaction was maintained at 0 °C for 2 h and transferred to room temperature for another 24 h. The viscous solution obtained was slowly poured into methanol/water (v/v = 1/1) mixed solvent. The precipitates collected were washed repeatedly and dried under vacuum to give FPHA. ^1H NMR (400 MHz, DMSO- d_6 , δ): 10.37 ppm (s, 2H, N—H); 9.71 ppm (s, 2H, O—H); 8.07–8.04 ppm (m, 4H, Ar—H); 7.92–7.88 ppm (m, 2H, Ar—H); 7.06–6.97 ppm (m, 4H, Ar—H).

2.4. Preparation of FG/FPBO composite films

The synthesis procedure of FG/FPBO composite films is illustrated in Fig. 1 b. FPHA was dissolved in the NMP dispersion of FG and stirred vigorously for 12 h to obtain a homogeneous mixture with the FPHA

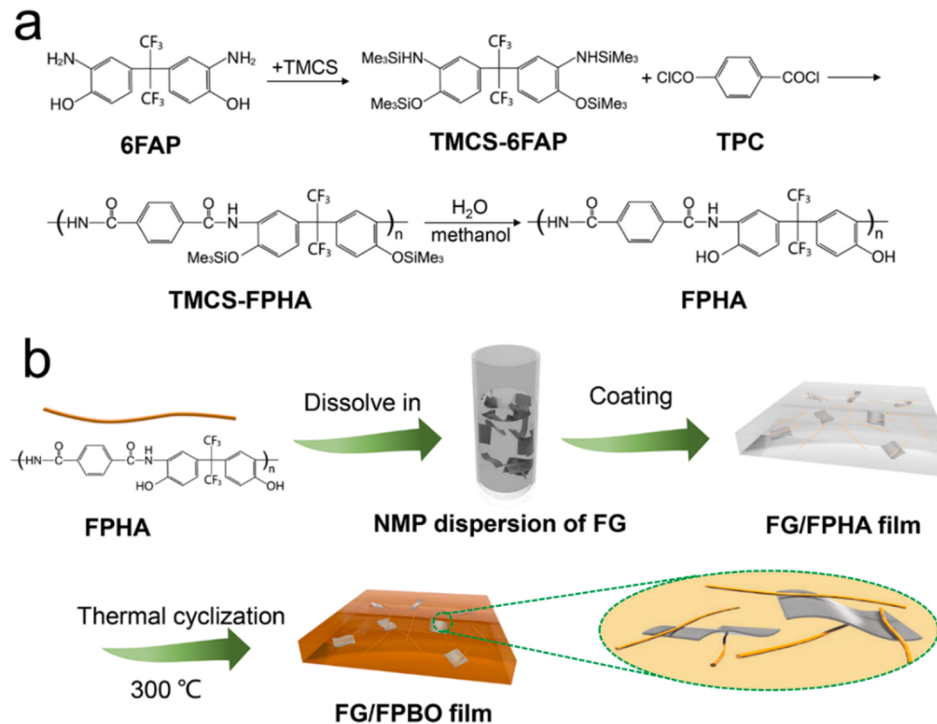


Fig. 1. Synthetic route of FPHA (a) and FG/FPBO composite films (b). (For interpretation of the references to colour in this figure legend, the reader is referred to the web version of this article.)

concentration of 15 wt%. The mixture was coated on a glass plate and kept at 60 °C for 4 h to form a film. Subsequently, the film was dried at 180 °C for 4 h under vacuum to remove the residual solvent. The FG/FPHA film obtained was further treated at 300 °C under nitrogen atmosphere for 4 h to convert to FG/FPBO. The resulting films with FG content of 0, 0.1, 0.3, 0.6, and 1.0 wt% were denoted as pristine FPBO, FG_{0.1}/FPBO, FG_{0.3}/FPBO, FG_{0.6}/FPBO, and FG_{1.0}/FPBO, respectively. The thickness of the films was controlled at 33–35 μm.

2.5. Characterization

The morphology of FG was observed by Hitachi HT7700 transmission electron microscope (TEM) and Bruker multimode 8 atomic force microscope (AFM). X-ray photoelectron spectroscopy (XPS) measurements were performed on the Thermo Scientific ESCALab 250Xi from VG instruments using 200 W monochromated Al K α radiation. The proton nuclear magnetic resonance (¹H NMR) spectra of the precursor FPHA was measured on a Bruker Avance III (400 MHz) with deuterated dimethylsulfoxide (DMSO-d₆) as the solvent. The intrinsic viscosity of FPHA was measured with a concentration of 0.5 g/dL in NMP using an Ubbelohde viscometer at 30 °C. The intrinsic viscosity is calculated by the formula of viscosity and molecular weight of polymer in GB/T 14190-93:

$$\eta_r = \frac{t_1}{t_0} \quad (1)$$

$$\eta_{sp} = \frac{t_1 - t_0}{t_0} \quad (2)$$

$$[\eta] = \frac{\sqrt{1 + 1.4\eta_{sp}} - 1}{0.7c} \quad (3)$$

where η_r is the relative viscosity, η_{sp} is the specific viscosity, t_0 is the outflow time of solvent, t_1 is the outflow time of solution, and c is the solution concentration.

The Fourier transform infrared spectrum (ATR-FTIR) of the composite films were obtained by a Nicolet 6700 Fourier transform infrared spectrometer with an attenuated total reflection device (smart orbit) at room temperature. The test wavenumber range was 4000–650 cm⁻¹, and the resolution was 4.0 cm⁻¹. X-ray diffraction (XRD) was measured by PANalytical Empyrean X-ray diffractometer with Cu-K α as the ray source ($\lambda = 0.154$ nm), the scanning voltage and current were 40 kV and 40 mA respectively, and the scanning range was 2–40°. Thermogravimetric analysis (TGA) was carried out by PerkinElmer TGA 8000 in nitrogen atmosphere. The thermogravimetric curves of the composite films were obtained by heating from 50 °C to 800 °C at a heating rate of 20 °C/min. The dielectric constant and dielectric loss of the composite films were determined by Novocontrol concept 40 dielectric impedance spectroscopy in the range of 10²–10⁷ Hz. The mechanical properties of the composite films were tested by Instron 3365 universal tensile testing machine. The sample was cut into a 40 × 10 mm strip according to the tensile standard, and the tensile rate was 2 mm/min. The final result is the average of five times tensile data. Statistical differences of tensile strength and tensile modulus were determined using Kruskal-Wallis tests, and significance levels were set at $P < 0.05$. The fracture surface morphology of the films after stretching was observed by JSM-6700F field emission scanning electron microscope (SEM) with electron acceleration voltage at 5 kV, and the samples were sprayed with gold before observation. The surface elemental mappings were acquired by another SEM (SU1510, Hitachi High-Tech Corporation) equipped with an electron-dispersive X-ray spectroscope (EDS). The water absorption rate of the composite films was measured by immersing the dry composite films in deionized water and calculating the mass change of the films for 12–72 h. The contact angle of water on the composite films was measured using an optical contact angle meter from DataPhysics Instruments.

3. Results and discussions

3.1. Preparation and characterization of FG

Liquid-phase exfoliation has been proven to be an effective method for the preparation of high-quality FG. Due to the matching of surface energy, IPA solvent can easily intercalate into the interlayers of graphite fluoride and greatly facilitate the exfoliation with the aid of sonication [32]. The IPA in the supernatant was replaced with NMP. As shown in Fig. 2a-c, the exfoliated FG can be stably dispersed in NMP and exhibit a strong Tyndall effect for at least one week. The morphology of FG was first observed by TEM. As shown in Fig. 2c-e, the obtained FG presented as transparent nanosheets with a size of 0.5–2 μm. The time of ultrasonic exfoliation has a significant effect on the morphology of FG. Due to the strong cavitation, the size of FG sheets apparently decreased with the increase of sonication time (Fig. S1). XPS spectroscopy was applied to explore the change in chemical structure of FG before and after ultrasonic exfoliation. As Table 1 shows, the graphite fluoride was composed of C and F elements in a ratio of 1:1.18. Traces of O element may originate from oxidation at the edges of the carbon network. However, a clear decrease in F content was observed during the sonication process, which suggested the departure of fluorine from FG. After 24 h of ultrasonic treatment, the content of F atoms dropped from 53.64% to 40.85%, and the C/F atomic ratio increased to 1:0.74. The removal of F atoms will inevitably impair the excellent dielectric properties of FG. Indeed, as the sonication time increased, the dielectric and mechanical properties of FG/FPBO composite decreased (Fig. S2). Therefore, FG with ultrasonic peeling for 6 h was carefully selected for follow-up researches. The thickness of FG was further measured by AFM. The result (Fig. 2 f) shows that the exfoliated FG nanosheets have a thickness of approximately 3–4 nm. Hence, the AFM and TEM results provided strong evidence for the successful preparation of two-dimensional FG.

3.2. Synthesis and characterization of FPBA

The insolubility of rigid PBO molecules in most organic solvents, as well as the absence of a melting temperature, greatly hinders the fabrication of PBO films. Therefore, a two-step strategy has been developed, including the preparation of PHA precursor films followed by ring-closing to PBO films. To improve the solubility of PHA, a fluorine-containing monomer of 6FAP was selected. Meanwhile, the pendant hydroxy groups of 6FAP were protected by trimethylsilyl groups before polymerization to obtain a high-molecular-weight linear PHA. The chemical structure of the synthesized FPBA was characterized by ¹H NMR. As shown in Fig. 3 a, the signals of aromatic protons in residues of 6FAP appeared at 7.06 and 7.92 ppm. The peak at 8.07 ppm could be assigned to the protons in residues of TPC. Other signals at 10.37 and 9.71 ppm with an integral ratio of 1:1 were attributed to the protons of —OH and —NH—, which confirmed the linear structure of the FPBA. In addition, the synthesized FPBA could well dissolved in NMP, and its intrinsic viscosity was determined to be 1.06 dL/g, which is high enough for the preparation of mechanically robust films [21].

The FPBA films could be further converted into FPBO films through a thermally induced ring-closing reaction. ATR-FTIR was used to monitor the change of chemical structures of the films before and after thermal treatment. As Fig. 3 b shows, a wide characteristic peak at around 3000–3500 cm⁻¹ could be observed in the spectrum of the precursor FPBA, which represented the stretching vibration of O—H and N—H. Besides, a characteristic peak occurred at 1650 cm⁻¹ can be ascribed to the stretching vibration of amide bond. However, these peaks disappeared after the thermal cyclization. Instead, a new peak attributed to the stretching of oxazole ring could be found at 1620 cm⁻¹, which suggested the formation of benzoxazole structure and the successful conversion of FPBA to FPBO.

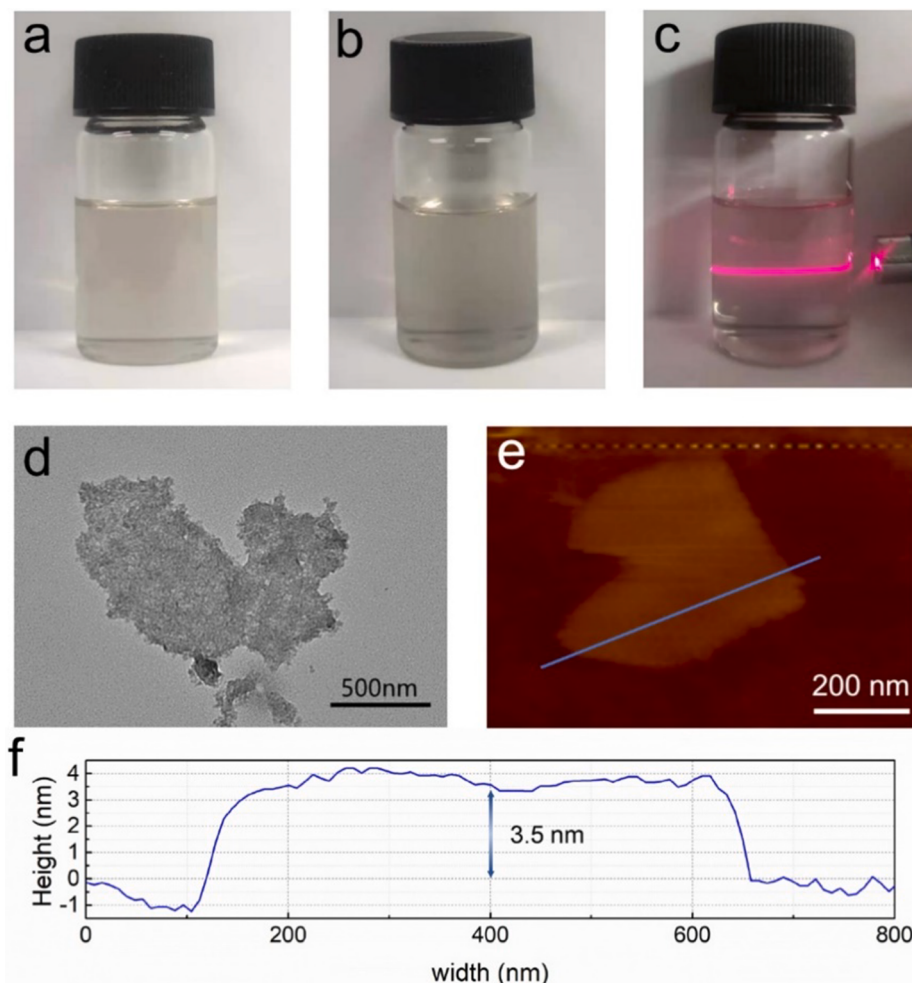


Fig. 2. Photos of FG dispersions placed for 0 (a) and 7 days (b). Tyndall effect of the FG dispersion (c). TEM (d) and AFM (e) images of FG with exfoliation for 6 h. Height and width of the FG nanosheet in AFM image (f). (For interpretation of the references to colour in this figure legend, the reader is referred to the web version of this article.)

Table 1
Content of each element in FG and graphite fluoride.

	C	F	O	C:F
graphite fluoride	45.35	53.64	1.02	1:1.18
FG (6 h)	51.85	47.11	1.04	1:0.90
FG (12 h)	51.69	45.39	2.92	1:0.87
FG (24 h)	54.78	40.85	4.36	1:0.74

3.3. Microstructure of FG/FPBO composite films

The uniform dispersion of FG in the polymer matrix is necessary for the fabrication of composite films with excellent properties. The π - π interaction between benzoxazole ring and carbon network, as well as the fluorine-containing groups in the backbone of FPBO, greatly improved the interfacial compatibility between FG and FPBO [33]. As shown in Fig. 4 b, FG can stably exist in the PHA solution for a long time without precipitation. Thus, transparent and homogeneous films (Fig. 4 a) could be obtained by casting. The dispersion of FG in FPBO matrix was examined by XRD, and the result was presented in Fig. 4 c. For comparison, graphite fluoride/FPBO composite films were prepared by the same method as FG/FPBO. Obviously, the pattern of graphite fluoride/FPBO exhibited two obvious diffraction peaks at 13.5° and 25.5°, which were assigned to (001) and (002) reflection of graphite fluoride [34]. However, all the sharp peaks disappeared on the pattern of the FG_{0.6}/

FPBO, indicating that the layered structure of graphite fluoride was completely destroyed after ultrasonic exfoliation, and the exfoliated FG was uniformly dispersed in the FPBO matrix without obvious reaggregation. Furthermore, the influence of the introduction of FG on the structure of FPBO was also studied by XRD. In Fig. 4 d, a wide characteristic diffraction peak could be observed at 15.5° for pristine FPBO. However, for FG/FPBO composites, the intensity of diffraction peak at 15.5° decreased gradually as the FG content increased. This could be attributed to the fact that FG was inserted between the molecular chains of FPBO, hindering the arrangement of the molecular chains and reducing their packing density. In contrast, the ATR-FTIR spectra of the composite films showed little difference from that of pristine FPBO, suggesting that the introduction of FG will not affect the ring-closing reaction of FPHA.

3.4. Thermal properties

The heat resistance of the FPBO films was tested by TGA in N₂ atmosphere, and the results were shown in Fig. 5 and Table 2. As expected, the inert ladder-like rigid structure endows FPBO with excellent thermal stabilities. The pristine FPBO films showed 5% weight loss (t₅) at 523 °C, and 10% weight loss (t₁₀) at 561 °C, which further confirmed the complete cyclization of FPHA during the thermal treatment. The slight weight loss below 500 °C could be attributed to the evaporation of absorbed moisture and residual solvent. Similar to FPBO, FG showed

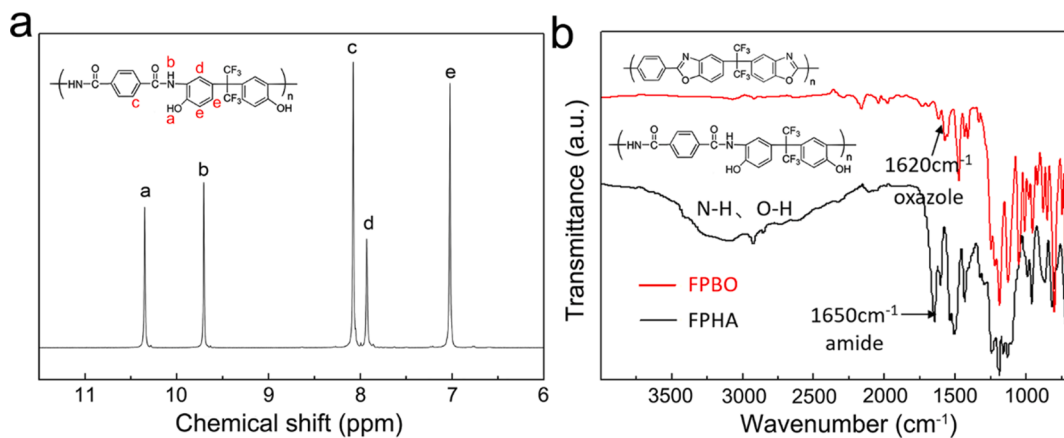


Fig. 3. ¹H NMR spectra of FPHA (a). ATR-FTIR spectra of FPHA and FPBO (b). (For interpretation of the references to colour in this figure legend, the reader is referred to the web version of this article.)

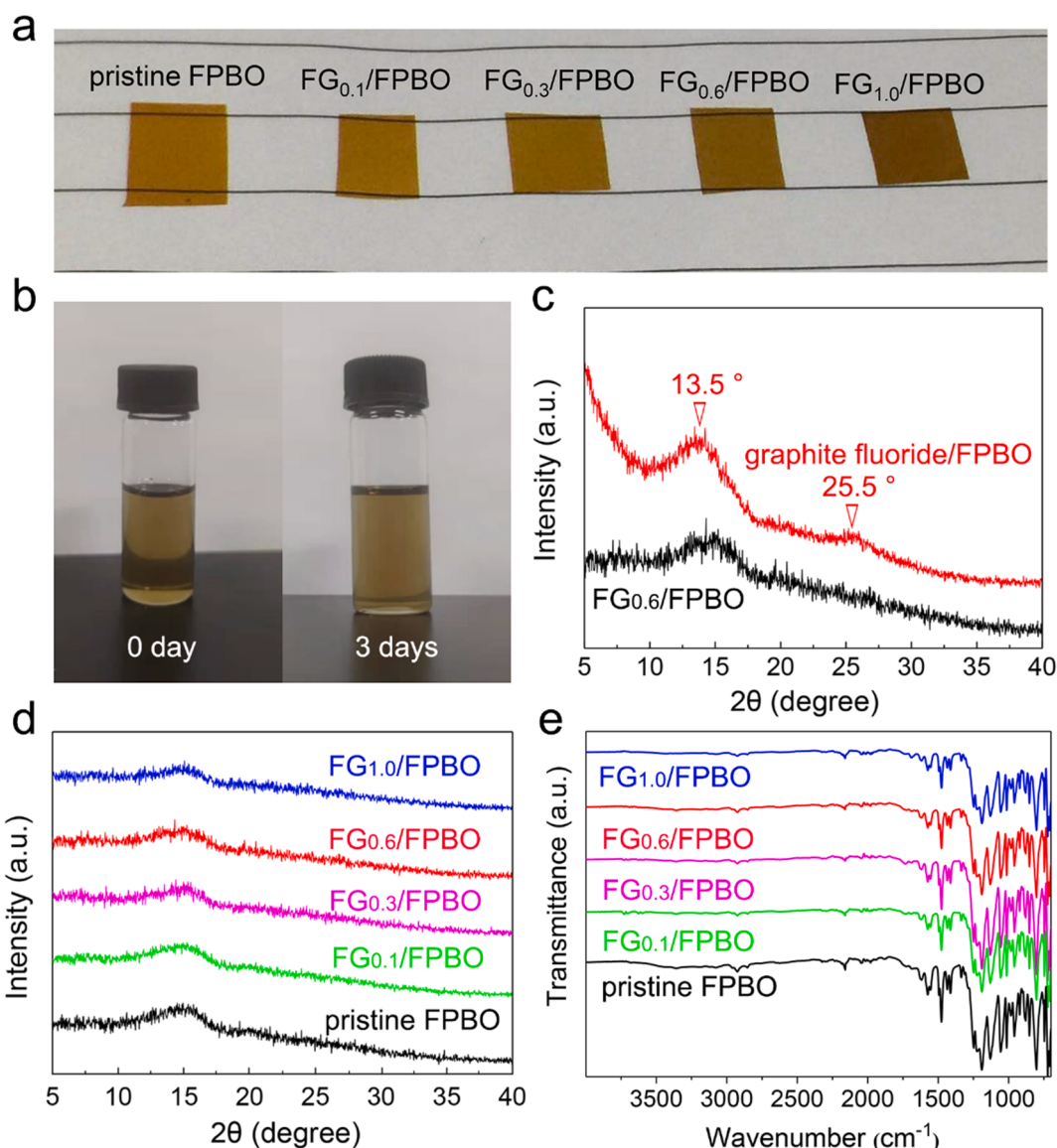


Fig. 4. Photos of pristine FPBO and FG/FPBO composite films (a). FPHA solution with 0.6 wt% FG, placed for 0 and 3 days (b). XRD patterns (c, d) and ATR-FTIR spectra (e) of composite films. (For interpretation of the references to colour in this figure legend, the reader is referred to the web version of this article.)

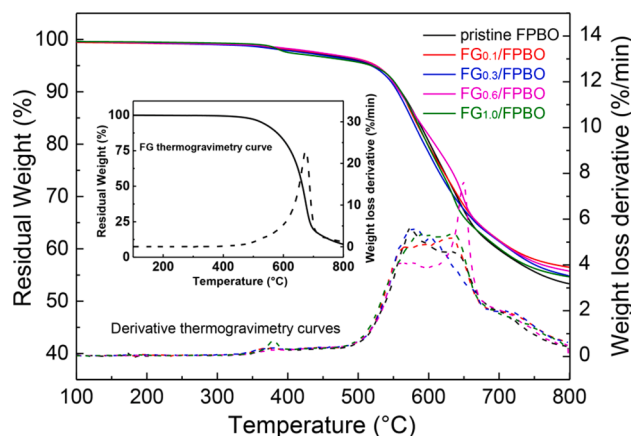


Fig. 5. Thermogravimetry and derivative curves of FG and composite films. (For interpretation of the references to colour in this figure legend, the reader is referred to the web version of this article.)

Table 2
Weight loss temperature of pristine and composite films.

	t ₅ (°C)	t ₁₀ (°C)	t _{onset} (°C)	t _{max} (°C)	Weight loss rate at 800 °C (%)
pristine FPBO	523	561	546	605	46.7
FG0.1/FPBO	525	560	535	608	43.5
FG0.3/FPBO	518	556	541	601	45.1
FG0.6/FPBO	524	559	537	610	44.2
FG1.0/FPBO	513	555	537	602	45.5

little weight loss below 500 °C due to the absence of easily thermally decomposable groups. Therefore, with the introduction of FG, the thermogravimetric curves of the composite films did not change significantly compared with that of the pristine FPBO. This indicated that the FG/FPBO composite films maintained the original superb heat resistance of FPBO.

3.5. Dielectric properties

Dielectric properties are the key factors that determine the application of a material in the field of electronic packaging. The dielectric constant and loss tangent were measured to evaluate the dielectric properties of FPBO films. As shown in the Fig. 6 a, the pristine FPBO had a dielectric constant of 2.71 at 1 MHz and room temperature, which was slightly lower than that of other PBO-based derivatives due to the incorporation of the trifluoromethyl groups with low polarizability. The introduction of FG into FPBO led to a further decrease in its dielectric constant. Moreover, the dielectric constant of the FG/FPBO films dropped sharply as the FG content increased. A minimum value of 2.02 could be achieved when FG increased to 1 wt%. However, the dielectric constant increased slightly as the test frequency decreased. This can be owed to the fact that the dipoles were aligned under the action of an external electric field at low frequencies, which resulted in relaxation polarization and thus an increase in dielectric constant. The relaxation polarization would be less apparent when the frequency increased, due to the delayed inversion of the dipole under the inner resistance of the material [35,36].

It was worth noting that more than 10 wt%, or even 20 wt% of low- κ nanofillers should be incorporated to greatly reduce the dielectric constant of PBO in previous studies [12,21]. Therefore, compared with previous reported low- κ nanofillers, FG used in this work showed a higher efficiency. The low dielectric properties of FG/FPBO films were mainly attributed to the uniform dispersion of FG nanosheets in the

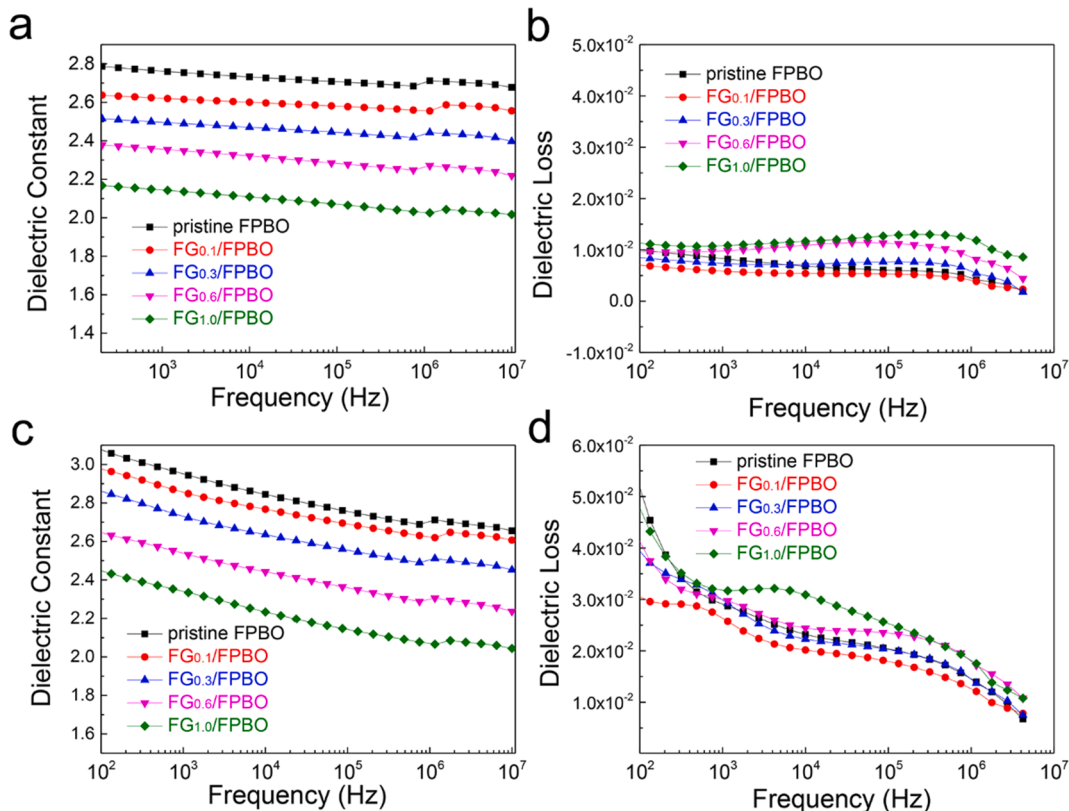


Fig. 6. Dielectric constant and dielectric loss of the composite films at room temperature (a, b) and 200 °C (c, d). (For interpretation of the references to colour in this figure legend, the reader is referred to the web version of this article.)

FPBO matrix, which inhibited the regular arrangement and orientation of FPBO molecular chains, thereby reducing the dipolar polarization caused by charge transfer between FPBO molecules. In addition, the abundant C-F bonds in FG contributed to reducing the polarizability of the composite films, which was another way to effectively reduce the dielectric constant.

The energy dissipation generated during the dipolar polarization can be characterized by the dielectric loss tangent. As shown in Fig. 6 b, the loss tangent of the composite films was kept at a low level of about 0.01 at the test frequencies, which agreed well with the result of dielectric constant, indicating the high efficiency of FG. Interestingly, the composite films can maintain a low dielectric loss and only observed a slight increase under the high content of FG, which may be caused by the interfacial polarization.

The stability of dielectric properties at high temperatures will be particularly important for electronic components worked in extreme environments. Therefore, the dielectric properties of the FG/FPBO composite films at 200 °C were measured, as shown in the Fig. 6 c and d. Apparently, the change of the dielectric constant and loss tangent at 200 °C showed a similar trend to those at room temperature. Although a slight increase could be detected at 200 °C, the dielectric constant and loss tangent of FG/FPBO composite films still maintained at an extremely low level compared with those of other organic low- κ materials [37,38]. Therefore, the excellent dielectric properties of the FG/FPBO composite film both at room and high temperature made it a promising low- κ material for application under extreme working conditions.

3.6. Mechanical properties

Apart from dielectric properties, the mechanical properties are also greatly important for interlayer dielectric materials. Unfortunately, in previous studies, the excessive addition of dielectric nanofillers greatly reduced the mechanical strength of resulting composites as well due to the severe aggregation of nanofillers. In sharp contrast, the mechanical properties of the FPBO films improved gradually with the increase of FG content. As Fig. 7 shows, the tensile strength and modulus increased from 82.6 MPa and 1.98 GPa to 103.5 MPa and 2.29 GPa, respectively. The outstanding mechanical properties could be owed to the uniform dispersion of FG in FPBO matrix, as well as the excellent interfacial compatibility which effectively improved the stress transfer at the interface.

The morphology of the fracture surface of the films after stretching was observed by SEM. It can be seen from the photos in Fig. 8 that the composite films all presented a single-phase structure without obvious phase separation. The EDS maps (Fig. S3) showed that the C and F

elements on the original film and the composite films all presented the same distribution, which indicated that no obvious agglomeration occurred. The fracture surface of pristine FPBO film was rather smooth, with few stripes and grooves. However, with the increase of the FG content, the roughness of the fracture surface increased significantly, which revealed the enhanced interaction between FPBO molecular chains and the transition of the fracture mechanism from brittleness to toughness. This result also provided solid evidence for the strong interfacial interaction between FG nanosheets and FPBO matrix. When the FG content reached up to 1.0 wt%, the tensile strength and modulus of the composite films decreased slightly, which might be resulted from the aggregation of FG in the matrix.

Although many subtle methods have been developed to reduce the dielectric constant of PBO, it is still a major challenge to simultaneously improve its mechanical properties. What is more, the decrease of the dielectric constant of PBO always comes at the expense of its excellent mechanical properties. As shown in Table 3, the tensile strength of the previous reported PBO-based nanocomposite or porous materials is generally less than 50 MPa. In contrast, the FG/FPBO composite films prepared in this work not only has a lower dielectric constant, but also has better mechanical properties.

3.7. Hydrophobic properties

Absorbing moisture will seriously reduce the reliability of insulating packaging materials, such as the deterioration of mechanical and dielectric properties, and even short circuits [39,40]. Polyimide, as a traditional insulating material, suffers greatly from a high water absorption (1–3%) due to the presence of polar carbonyl groups [12,41]. As an alternative, FPBO has a lower water absorption, which could be further reduced by the introduction of highly hydrophobic FG. As shown in Fig. 9 a, the saturated water absorption after 72 h has dropped from ~1% for pristine FPBO to only 0.5% for FG_{1.0}/FPBO. The water contact angle of the composite films is shown in Fig. 9 b. The contact angle increased with the increase of the FG content in the composite films. The contact angle of the composite film with 1.0 wt% FG reached 83.7 ± 1°, which indicated that FG can significantly improve the hydrophobicity of the film. The composite films with improved hydrophobicity are more conducive to the application in the field of electronic packaging.

4. Conclusion

In this study, the FG/FPBO composite films were successfully prepared by blending FPHA with FG, and subsequent thermal cyclization. The few-layered FG nanosheets with large aspect ratio were facilely prepared by ultrasonic exfoliation. Excitingly, the dielectric and mechanical properties of FPBO can be significantly improved by introducing a tiny amount of FG. At 1 MHz and room temperature, the dielectric constant of FG_{1.0}/FPBO was 2.02, which was 25.5% lower than that of the pure FPBO. The excellent dielectric properties could be well maintained even at a high temperature. Thanks to the uniform dispersion of FG in FPBO matrix and the excellent interfacial compatibility, the tensile strength and modulus of the FG/FPBO films greatly increased to 103.5 MPa and 2.29 GPa from 82.6 MPa and 1.98 GPa of pure FPBO, respectively. Moreover, the composite films possessed outstanding thermal stability with the 5% weight loss temperature as high as 525 °C. Owing to the highly hydrophobic nature of FG, the water absorption of the composite films has dropped by nearly 50% compared with that of pure FPBO. In summary, the FG_{1.0}/PBO composite film has the best comprehensive performance, such as the lowest dielectric constant and water absorption, as well as ultra-high mechanical and thermal properties. These properties indicate the composite film is a very promising insulating material to be employed in the fabrication of large-scale integrated circuits.

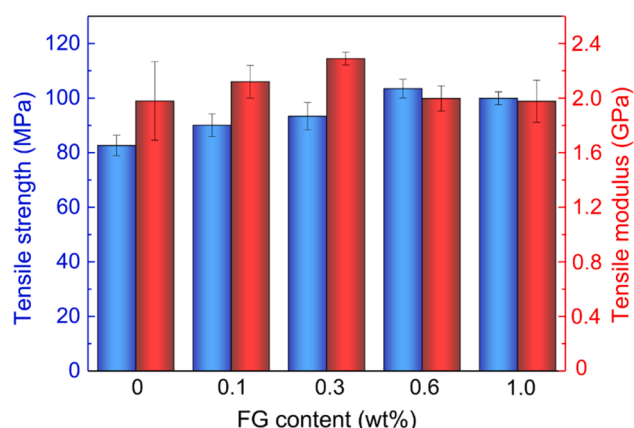


Fig. 7. Tensile strength and tensile modulus of the FG/FPBO composite films. (For interpretation of the references to colour in this figure legend, the reader is referred to the web version of this article.)

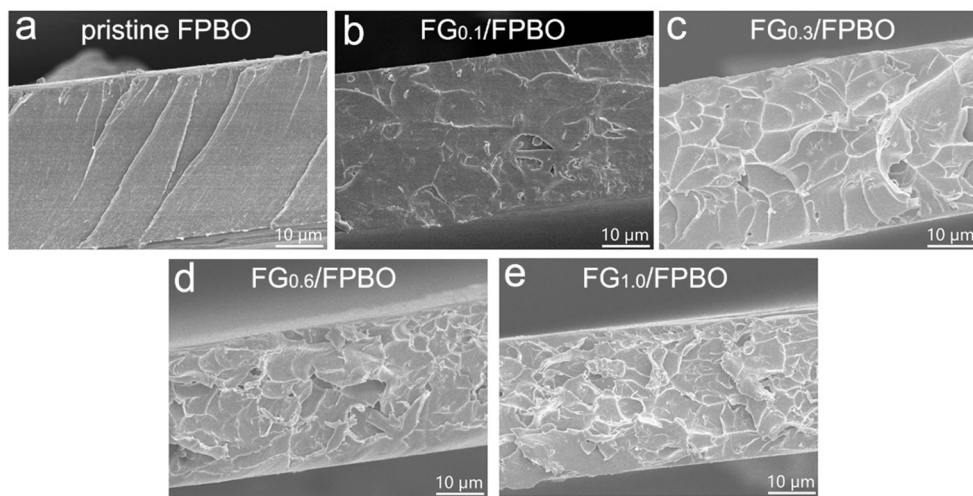


Fig. 8. SEM images of fracture surface of pristine FPBO (a), FG_{0.1}/FPBO (b), FG_{0.3}/FPBO (c), FG_{0.6}/FPBO (d) and FG_{1.0}/FPBO (e) composite films.

Table 3

Comparison of our results with the previous reports on tensile strength and dielectric constant.

Ref.	Material	Content (wt%)	Polymer matrix	nanofiller	
				Tensile strength (MPa)	Dielectric constant
This work	FG	1	FPBO	100	2.02
[21]	HMS@ZIF-8	8	FPBO	34	2.12
[19]	Microporous	32	PBO	16	2.37
[12]	hyperbranched PBO	20	FPBO	54	2.13
[6]	–	–	PBO-co-PBI	38	2.2
[4]	–	–	PI-co-PBO	50	2.56

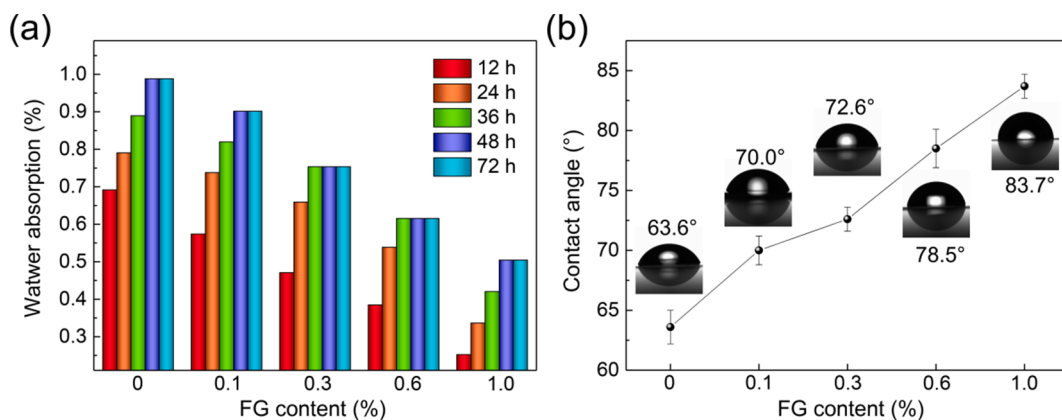


Fig. 9. Water absorption (a) and contact angle (b) of the FG/FPBO composite films. (For interpretation of the references to colour in this figure legend, the reader is referred to the web version of this article.)

CRediT authorship contribution statement

Zihua Yu: Investigation, Methodology, Writing - original draft.
Shaohua Wu: Investigation, Writing - review & editing, Funding acquisition.
Chuncheng Li: Supervision, Writing - review & editing.
Yaonan Xiao: Investigation, Visualization. **Liuchun Zheng:** Visualization.
Jiajian Liu: Validation. **Bo Zhang:** Investigation.

Declaration of Competing Interest

The authors declare that they have no known competing financial interests or personal relationships that could have appeared to influence the work reported in this paper.

Acknowledgements

Financial support from National Natural Science Foundation of China (Grant No. 51903237) is gratefully acknowledged. Thanks Dr. Hualin Ou from *Fantastic Color Animation Technology Co., Ltd.* for the designs of the illustration in this paper. The authors would like to thank the anonymous reviewers and the editor for their comments and suggestions which are extremely helpful for improving the quality of this paper.

Appendix A. Supplementary material

Supplementary data to this article can be found online at <https://doi.org/10.1016/j.compositesa.2021.106387>.

References

- [1] Yang D, Ni Y, Kong X, Gao D, Wang Y, Hu T, et al. Mussel-inspired modification of boron nitride for natural rubber composites with high thermal conductivity and low dielectric constant. *Compos Sci Technol* 2019;177:18–25. <https://doi.org/10.1016/j.compscitech.2019.04.016>.
- [2] Yuan C, Jin K, Li K, Diao S, Tong J, Fang Q. Non-porous low-k dielectric films based on a new structural amorphous fluoropolymer. *Adv Mater* 2013;25(35):4875–8. <https://doi.org/10.1002/adma.201302021>.
- [3] Kou Y, Zhou W, Li B, Dong L, Duan Y-E, Hou Q, et al. Enhanced mechanical and dielectric properties of an epoxy resin modified with hydroxyl-terminated polybutadiene. *Compos Part A-Appl S* 2018;114:97–106. <https://doi.org/10.1016/j.compositesa.2018.08.016c>.
- [4] Li X, Liu T, Jiao Y, Dong J, Gan F, Zhao X, et al. Novel high-performance poly(benzoxazole-co-imide) resins with low dielectric constants and superior thermal stabilities derived from thermal rearrangement of ortho-hydroxy polyimide oligomers. *Chem Eng J* 2019;359:641–51. <https://doi.org/10.1016/j.cej.2018.11.175>.
- [5] Zhao W, Kong J, Liu H, Zhuang Q, Gu J, Guo Z. Ultra-high thermally conductive and rapid heat responsive poly(benzobisoxazole) nanocomposites with self-aligned graphene. *Nanoscale* 2016;8(48):19984–93. <https://doi.org/10.1039/c6nr06622d>.
- [6] Nag A, Ali MA, Watanabe M, Singh M, Amornwachirabodee K, Kato S, et al. High-performance poly(benzoxazole/benzimidazole) bio-based plastics with ultra-low dielectric constant from 3-amino-4-hydroxybenzoic acid. *Polym Degrad Stab* 2019; 162:29–35. <https://doi.org/10.1016/j.polymdegradstab.2019.01.036>.
- [7] Qian Z, Yang M, Li R, Li D, Zhang J, Xiao Y, et al. Fire-resistant, ultralight, superelastic and thermally insulated polybenzazole aerogels. *J Mater Chem A* 2018;6(42):20769–77. <https://doi.org/10.1039/C8TA07204C>.
- [8] Hu Z, Li N, Li J, Zhang C, Song Y, Li X, et al. Facile preparation of poly(p-phenylene benzobisoxazole)/graphene composite films via one-pot in situ polymerization. *Polymer* 2015;71:8–14. <https://doi.org/10.1016/j.polymer.2015.06.047>.
- [9] Fukumaru T, Fujigaya T, Nakashima N. Extremely high thermal resistive poly(p-phenylene benzobisoxazole) with desired shape and form from a newly synthesized soluble precursor. *Macromolecules* 2012;45(10):4247–53. <https://doi.org/10.1021/ma3006256>.
- [10] Chen M, Wu Y, Song W, Mo Y, Lin X, He Q, et al. Plasmonic nanoparticle-embedded poly(p-phenylene benzobisoxazole) nanofibrous composite films for solar steam generation. *Nanoscale* 2018;10(13):6186–93. <https://doi.org/10.1039/C8NR01017J>.
- [11] Shin SW, Kim JS, Kim SJ, Kim DW, Jung HT. Polybenzoxazole/graphene nanocomposite for etching hardmask. *J Ind Eng Chem* 2019;75:296–303. <https://doi.org/10.1016/j.jiec.2019.03.042>.
- [12] Wang Y, Yu J, Zhu J, Hu Z. Hyperbranched polybenzoxazoles incorporated polybenzoxazoles for high-performance and low-K materials. *J Polym Sci, Part A: Polym Chem* 2016;54(11):1623–32. <https://doi.org/10.1002/pola.28018>.
- [13] Volksen W, Miller RD, Dubois G. Low dielectric constant materials. *Chem Rev* 2010;110(1):56–110. <https://doi.org/10.1021/cr9002819>.
- [14] Si L, Guo D, Xie G, Luo J. Mechanical properties and interface characteristics of nanoporous low-k materials. *ACS Appl Mater Interfaces* 2014;6(16):13850–8. <https://doi.org/10.1021/am503236m>.
- [15] Long T, Swager T. Molecular design of free volume as a route to low-kappa dielectric materials. *J Am Chem Soc* 2003;125(46):14113–9. <https://doi.org/10.1021/ja0360945>.
- [16] Zhang P, Zhao J, Zhang Ke, Bai R, Wang Y, Hua C, et al. Fluorographene/polyimide composite films: Mechanical, electrical, hydrophobic, thermal and low dielectric properties. *Compos Part A-Appl S* 2016;84:428–34. <https://doi.org/10.1016/j.compositesa.2016.02.019>.
- [17] Bei R, Qian C, Zhang Yi, Chi Z, Liu S, Chen X, et al. Intrinsic low dielectric constant polyimides: relationship between molecular structure and dielectric properties. *J Mater Chem C* 2017;5(48):12807–15. <https://doi.org/10.1039/C7TC04220E>.
- [18] Wang L, Liu X, Liu C, Zhou X, Liu C, Cheng M, et al. Ultralow dielectric constant polyarylene ether nitrile foam with excellent mechanical properties. *Chem Eng J* 2020;384:123231. <https://doi.org/10.1016/j.cej.2019.123231>.
- [19] Fukumaru T, Fujigaya T, Nakashima N. Design and preparation of porous polybenzoxazole films using the tert-butoxycarbonyl group as a pore generator and their application for patternable low-k materials. *Polym Chem* 2012;3(2):369–76. <https://doi.org/10.1039/c1py00470k>.
- [20] Huang C, Li J, Xie G, Han F, Huang D, Zhang F, et al. Low-dielectric constant and low-temperature curable polyimide/POSS nanocomposites. *Macromol Mater Eng* 2019;304(12):1900505. <https://doi.org/10.1002/mame.201900505>.
- [21] Zhou X, Liu X, Cui Z, Gu J, Lin S, Zhuang Q. Design and development of HMS@ZIF-8 fluorinated polybenzoxazole composite films with excellent low-k performance, mechanical properties and thermal stability. *J Mater Chem C* 2020;8(22):7476–84. <https://doi.org/10.1039/d0tc00124d>.
- [22] Guo D, Jiang J, Liu Y, Liu X, Sheng S. New fluorinated xanthene-containing polybenzoxazoles with low dielectric constants. *J Fluorine Chem* 2015;175: 169–75. <https://doi.org/10.1016/j.jfluchem.2015.05.001>.
- [23] Dang TD, Mather PT, Alexander MD, Grayson CJ, Houtz MD, Spry RJ, et al. Synthesis and characterization of fluorinated benzoxazole polymers with high T-g and low dielectric constant. *J Polym Sci, Part A: Polym Chem* 2000;38(11): 1991–2003. [https://doi.org/10.1002/\(sici\)1099-0518\(20000601\)38:11<1991::aid-pola80>3.3.co;2-w](https://doi.org/10.1002/(sici)1099-0518(20000601)38:11<1991::aid-pola80>3.3.co;2-w).
- [24] Tao L, Yang H, Liu J, Fan L, Yang S. Synthesis of fluorinated polybenzoxazoles with low dielectric constants. *J Polym Sci, Part A: Polym Chem* 2010;48(21):4668–80. <https://doi.org/10.1002/pola.24253>.
- [25] Nair RR, Ren W, Jalil R, Riaz I, Kravets VG, Britnell L, et al. Fluorographene: a two-dimensional counterpart of Teflon. *Small* 2010;6(24):2877–84. <https://doi.org/10.1002/smll.201001555>.
- [26] Ye X, Liu X, Yang Z, Wang Z, Wang H, Wang J, et al. Tribological properties of fluorinated graphene reinforced polyimide composite coatings under different lubricated conditions. *Compos Part A-Appl S* 2016;81:282–8. <https://doi.org/10.1016/j.compositesa.2015.11.029>.
- [27] Samarakoon DK, Chen Z, Nicolas C, Wang XQ. Structural and electronic properties of fluorographene. *Small* 2011;7(7):965–9. <https://doi.org/10.1002/smll.201002058>.
- [28] Robinson JT, Burgess JS, Junkermeier CE, Badescu SC, Reinecke TL, Perkins FK, et al. Properties of fluorinated graphene films. *Nano Lett* 2010;10(8):3001–5. <https://doi.org/10.1021/nl101437p>.
- [29] Kwon S, Ko JH, Jeon KJ, Kim YH, Park JY. Enhanced nanoscale friction on fluorinated graphene. *Nano Lett* 2012;12(12):6043–8. <https://doi.org/10.1021/nl204019k>.
- [30] Gu J, Dong W, Xu S, Tang Y, Ye L, Kong J. Development of wave-transparent, lightweight composites combined with superior dielectric performance and desirable thermal stabilities. *Compos Sci Technol* 2017;144:185–92. <https://doi.org/10.1016/j.compscitech.2017.03.027>.
- [31] Chen Yi, Zhang S, Liu X, Pei Q, Qian J, Zhuang Q, et al. Preparation of solution-processable reduced graphene oxide/polybenzoxazole nanocomposites with improved dielectric properties. *Macromolecules* 2015;48(2):365–72. <https://doi.org/10.1021/ma502326v>.
- [32] Wang X, Wu P. Highly thermally conductive fluorinated graphene films with superior electrical insulation and mechanical flexibility. *ACS Appl Mater Interfaces* 2019;11(24):21946–54. <https://doi.org/10.1021/acsmami.9b07377>.
- [33] Wang Y, Xia S, Li H, Wang J. Unprecedentedly tough, folding-endurance, and multifunctional graphene-based artificial nacre with predesigned 3D nanofiber network as matrix. *Adv Funct Mater* 2019;29(38):1903876. <https://doi.org/10.1002/adfm.201903876>.
- [34] Kang W, Li S. Preparation of fluorinated graphene to study its gas sensitivity. *RSC Adv* 2018;8(41):23459–67. <https://doi.org/10.1039/c8ra03451f>.
- [35] Simpson JO, St Clair AK. Fundamental insight on developing low dielectric constant polyimides. *Thin Solid Films* 1997;308:480–5. [https://doi.org/10.1016/s0040-6090\(97\)00481-1](https://doi.org/10.1016/s0040-6090(97)00481-1).
- [36] Liu X, Sun H, Liu S, Jiang Y, Yu B, Ning N, et al. Mechanical, dielectric and actuated properties of carboxyl grafted silicone elastomer composites containing epoxy-functionalized TiO2 filler. *Chem Eng J* 2020;393:124791. <https://doi.org/10.1016/j.cej.2020.124791>.
- [37] Lin JJ, Wang XD. Novel low-kappa polyimide/mesoporous silica composite films: Preparation, microstructure, and properties. *Polymer* 2007;48(1):318–29. <https://doi.org/10.1016/j.polymer.2006.10.037>.
- [38] Lu Y, Zhang S, Geng Z, Du Y, Zhu K, Li Y, et al. Design and preparation of silica tube/poly(aryl ether ketone) composites with low dielectric constant. *RSC Adv* 2016;6(77):72999–3005. <https://doi.org/10.1039/C6RA13855A>.
- [39] Tan CM, Narula U, Seow GL, Sangwan V, Chen CH, Lin SP, et al. Moisture resistance evaluation on single electronic package moulding compound. *J Mater Chem C* 2020;8(6):1943–52. <https://doi.org/10.1039/C9TC04298A>.
- [40] Harsányi G. Irregular effect of chloride impurities on migration failure reliability: contradictions or understandable? *Microelectron Reliab* 1999;39(9):1407–11. [https://doi.org/10.1016/S0026-2714\(99\)00079-7](https://doi.org/10.1016/S0026-2714(99)00079-7).
- [41] Chern Y, Tsai J. Low dielectric constant and high organosolubility of novel polyimide derived from unsymmetric 1,4-Bis(4-aminophenoxy)-2,6-di-tert-butylbenzene. *Macromolecules* 2008;41(24):9556–64. <https://doi.org/10.1021/ma802305q>.